Special issue – Fan 2015

Institution of MECHANICAL ENGINEERS
Journal of POWER AND ENERGY

Proc IMechE Part A:
J Power and Energy
0(0) 1–15

DOI: 10.1177/0957650915626259
pia.sagepub.com
SAGE

Implementation of an acoustic stall detection system using near-field DIY pressure sensors

Alessandro Corsini[1,2], Cecilia Tortora[1], Sara Feudo[1], Anthony G Sheard[3] and Graziano Ullucci[2]

Abstract

In this paper, the use of DIY transducers is proposed to detect the pressure instabilities in a low-speed industrial axial fan. The authors aim is to detect rotating stall, a well-studied aerodynamic instability with a typical frequency that can be even lower than 10 Hz in low-speed industrial fans. Pressure transducers and piezoelectric sensors, such as microphones, in turbomachinery are used respectively in the near and far field as standard methods to perform time-resolved pressure measurements. Other classes of sensors, such as electret microphones, may be not suited for pressure measurements, especially in the ultrasound region because their cut-off frequency is about 20 Hz. In this study, the authors use a low-cost DIY technology, as alternative technology to stall detection, in comparison with a high precision piezoelectric sensor. The authors performed the pressure measurements using a dynamic transducer, a piezoresistive transducer, and a piezoelectric high sensitivity sensor that provides the measurement baseline. They implemented and set-up a measurement chain to identify the typical rotating stall pattern in low-speed axial fans. The results have been validated with respect to the state-of-the-art acoustic control techniques described in literature. The signals acquired using the two technologies are discussed using a combination of spectral and time-domain space reconstruction. The acoustic patterns obtained through the phase space reconstruction show that the DIY dynamic sensor is a good candidate solution for the rotating stall acoustic analysis.

Keywords

Low speed axial fan, phase space reconstruction, stall detection

Date received: 12 September 2015; accepted: 2 November 2015

Introduction

The prediction of aerodynamic instabilities, such as rotating stall, is an important topic, relevant to design and operation of industrial turbomachinery. In the past decades, Emmons's[1] was one of the first to attempt in describing the mechanism underlying stall propagation. Later the rotating stall, its inception, propagation, and control have been widely observed and studied in many works on axial flow compressors.[2–6]

One of the possible causes of rotating stall can be the presence of fouling or icing on rotor or stator blades and in general in the duct, leading to a reduction of the flow section and therefore a decrease of the flow rate. This promotes the formation of stall cells and the onset of surge in axial fans and compressors, due to the drop in mass flow rate and the increase of pressure ratio, in multistage turbomachines these last phenomena propagates downstream to the following stages.[7]

These phenomena are designers' primary interest as a consequence of the correlated vibrational issues, leading to fatigue breakage of rotor blades. In this respect, the continuous machine monitoring is considered to be a remedial strategy able to detect the instabilities to allow timely intervention.

This paper reports on the rotating stall identification by means of the sound pressure signals emitted from an industrial low-speed axial fan. The aerodynamic instability are hydrodynamically detectable in the near field and, acoustically, since each turbomachine emits noise due to the high-speed flow through the rotor and stator blades, the intensity of it being dependent on the rotational frequency and the blade count and clocking.[8,9] Any reduction in

[1]Dipartimento di Ingegneria Meccanica e Aerospaziale, Sapienza University of Rome, Rome, Italy
[2]SED Soluzioni per l'Energia e la Diagnostica, Ferentino (FR), Italy
[3]AGS Consulting Llc, Atlanta, GA, USA

Corresponding author:
Cecilia Tortora, Dipartimento di Ingegneria Meccanica e Aerospaziale, Sapienza University of Rome, Via Eudossiana 18, Rome, Italy.
Email: cecilia.tortora@uniroma1.it

the flow stability has as a consequence a change in the noise emitted.

The available technologies to detect pressure instabilities, customary of turbomachinery, are based on the piezoelectric effect used in high-frequency response pressure transducers[10] and condenser microphones.[11,12] The benefit in using this kind of sensors is the high sensitivity in a large frequency range, i.e. from mHz to 20 kHz or even more. However, stall-related rotating instabilities have a frequency response typically lower than 100 Hz. This circumstance motivates the attempt to develop a low-cost sensoring solution, following the recent development of electret-based measurement microphones exploiting the large diffusion of electret capsules in the multi-media market.[13–16] The approach used to address this line of work has been the use of unconventional DIY sensors for unsteady pressure measurements based on a piezoresistive pressure transducer and a commercial dynamic microphone capsule, for the latter case the working principle is based on the electromagnetic induction. The measurement chains were first tested in an acoustically insulated duct in order to characterise the DIY sensors with respect to a high sensitivity piezoelectric microphone baseline. The comparative validation is then completed on a low-speed industrial axial fan test-rig in a fully reverberant acoustic condition.

Table 1. Pressure transducer specifications.

Typical error with auto zero	2.5% (over + 10°C to + 60°C)
Maximum error without auto zero	6.25% (over + 10°C to + 60°C)
Sensitivity	1.0 V/kPa
Time response	1.0 ms
Maximum pressure (P1 > P2)	75 kPa

Frequency- and time-domain analyses were performed on the acquired signals, to compare the performance of measurement methodologies under scrutiny during stall detection. The signal processing includes the reconstructed phase space methodology to detect the non-linear dynamics of measured pressure signals, not recognisable during visual inspection.

Methodology

Pressure transducer

The piezoresistive pressure transducer is an integrated silicon pressure sensor on-chip signal conditioned, temperature compensated, and calibrated. It is a piezoresistive transducer that provides an analogue output signal proportional to the applied pressure. The pressure range is −2 to 2 kPa (−0.3 to 0.3 psi), the output is 0.5 to 4.5 V. In Table 1 are listed the pressure transducer specifications. Figure 1 shows the cross-sectional diagram of the pressure sensor and the differential configuration on the basic chip carrier.

The decoupling circuit shown in Figure 2 is needed for interfacing the integrated sensor to the A/D input, and to comply with the sensor specifications.

Dynamic microphone

The DIY microphone used in the study is a commercial dynamic microphone. Table 2 gives the microphone characteristics.

Table 2. Microphone specifications.

Impedance	600 Ω ± 30 %
Sensitivity	−72 ± 3 dB
Frequency response	60–14 kHz

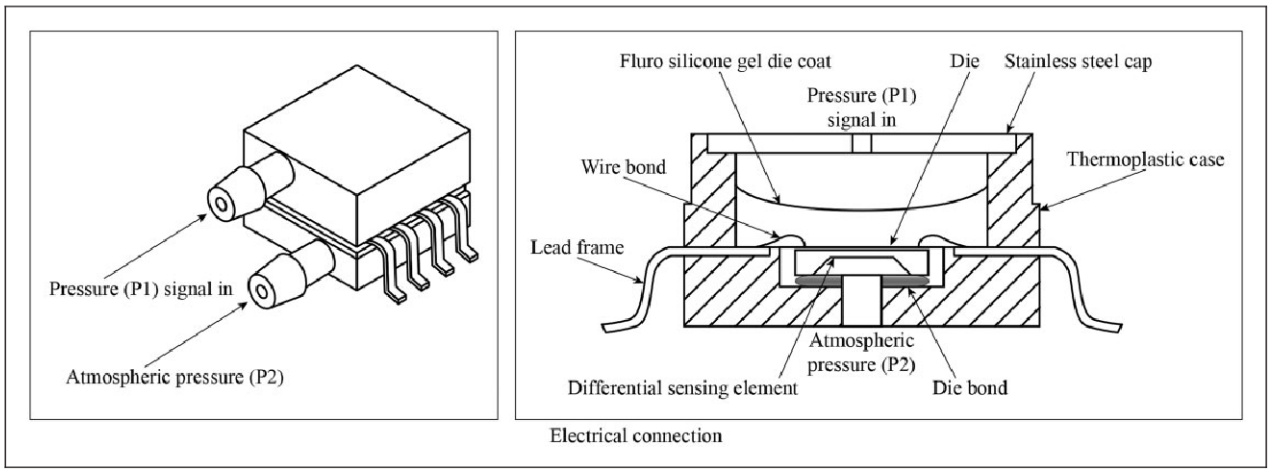

Figure 1. Pressure sensor and its cross-sectional diagram (not to scale).

The dynamic microphone operation is based on the electromagnetic induction: the motion of the internal components of the microphone generates a current output. The incoming sound pressure wave displaces a thin diaphragm, wrapped with a conductive coil of wire immersed in a magnetic field. The output is a voltage signal directly proportional to the sound pressure wave magnitude. The dynamic response is lower and the frequency response is less regular than ribbon or condenser microphones. The dynamic microphones are considered

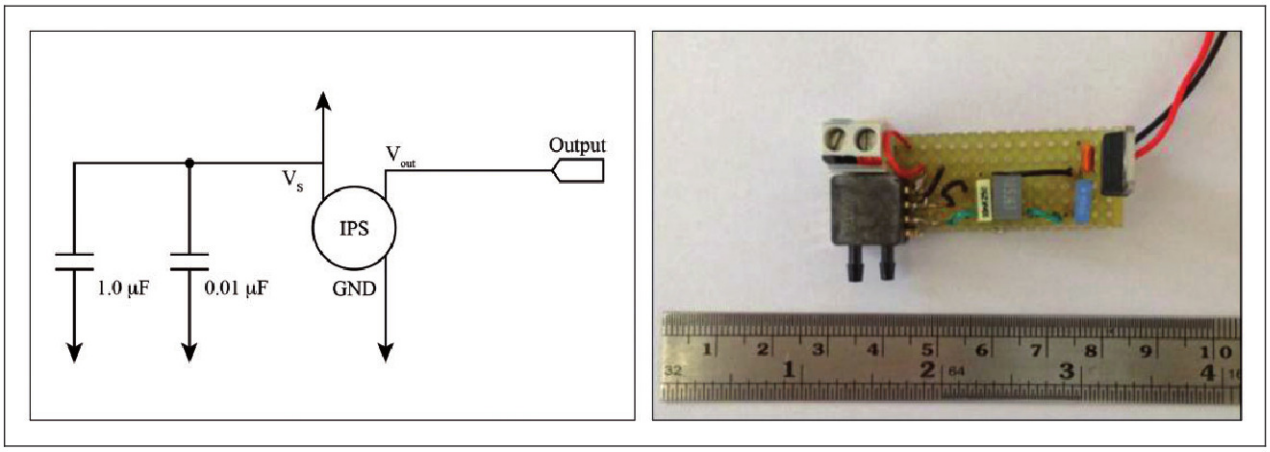

Figure 2. On the left: power supply decoupling and output filtering; on the right: pressure transducer final layout.

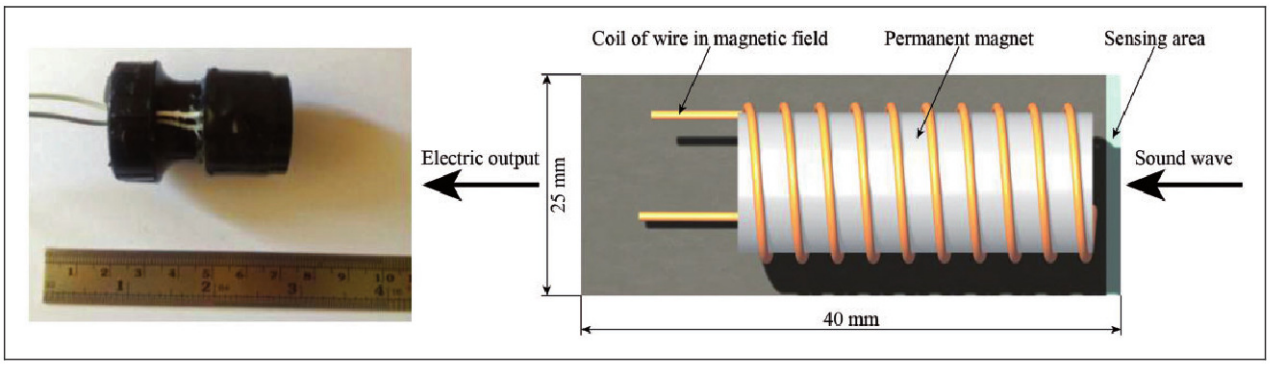

Figure 3. The dynamic microphone.

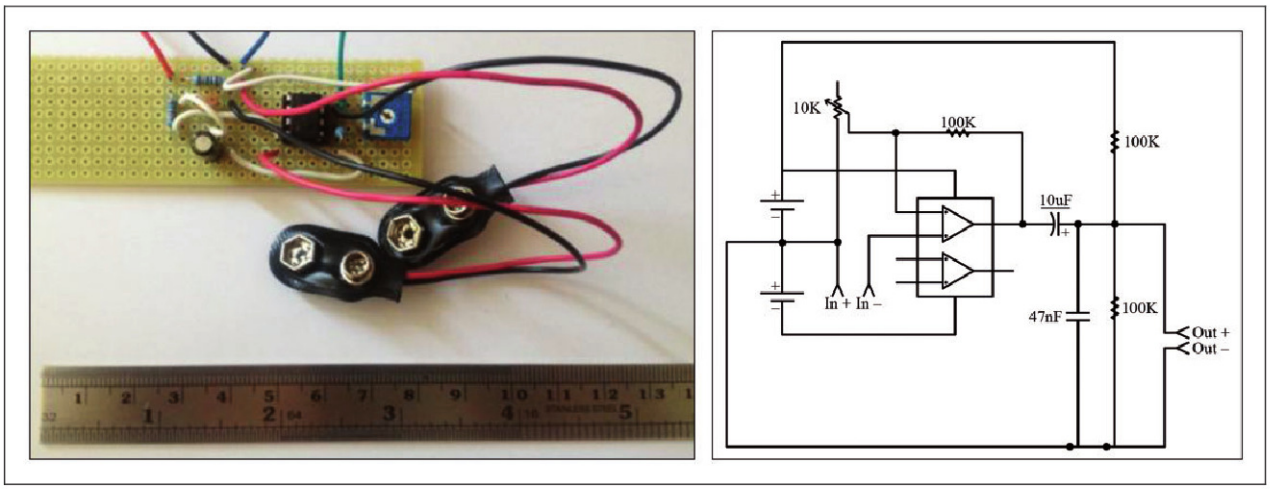

Figure 4. The amplifier circuit.

a solution to measure hydrodynamic pressure in the near field. They are used in harsh working conditions and high noise level, due to their resistance. Figure 3 shows the microphone capsule and its design concept.

Operational amplifier

The amplifier is needed for the dynamic microphone and the pressure transducer. The circuit is based on the TL082 operational amplifier arranged in a non-inverting architecture. The amplifier circuit showed in Figure 4 is powered by two 9 V batteries. A 10 kΩ linear potentiometer is set to the most suitable impedance for the connected sensor.

Piezoelectric microphone

The baseline probe is a high-precision pre-amplified piezoelectric condenser microphone calibrated and certified according to the ISO-9001. When used on a fan test-rig the piezoelectric microphone is usually placed in the far field. In Table 3 are shown the piezoelectric microphone characteristics.

Probe characterisation test-rig

To characterise the unconventional pressure transducers with respect to the piezoelectric microphone, the authors used an an-echoic rig with a termination equipped with a sound source, and the other termination was instrumented with the transducers and the microphone. The signals analysed are sine waves produced by a function generator; a set of frequencies were selected as the one closest to the pure tones of interest in the investigated axial fan. Figure 5 shows the layout of the characterisation rig.

The an-echoic tube was realised with a PVC duct with diameter 125 mm and length 500 mm. The duct was wrapped with foam to insulate it from the external noise. At one end of the duct was placed a loudspeaker with impedance of 8 Ω and maximum diameter of 125 mm. The loudspeaker was connected to the function generator. At the other end was placed a foam termination with inserted the pressure transducer and the piezoelectric microphone.

Function generator

The function generator typical outputs are sine waves, whose frequency and amplitude were regulated

Table 3. Piezoelectric microphone specifications.

Nominal microphone diameter	1/2"
Open-circuit sensitivity (at 250 Hz)	12.5 mV/Pa
Open-circuit sensitivity (±2 dB) (at 250 Hz)	−38.1 dB re 1 V/Pa
Frequency range (±2 dB)	4–20,000 Hz

Table 4. Function generator technical specifications.

Frequency range	0.2 Hz to 2 MHz
Output signal impedance	50 Ω
Output signal amplitude (peak–peak value)	Nonattenuate (2 Vp-p to 20 Vp-p) ± 20%[a] Attenuate 20 dB (0.2 Vp-p to 2.0 Vp-p) ± 20%[a] Attenuate 40 dB (20 mVp-p to 200 mVp-p) ± 20%[a]
Output signal features	Sine wave distortion < 2%[b]
Output signal frequency stability	Less than ± 0.1% / min[b]
Measurements errors	⩽ 0.5%

[a]Continuously adjustable.
[b]Test condition: frequency output 10 kHz, amplitude: 5 Vp-p, warm-up for 20 min.

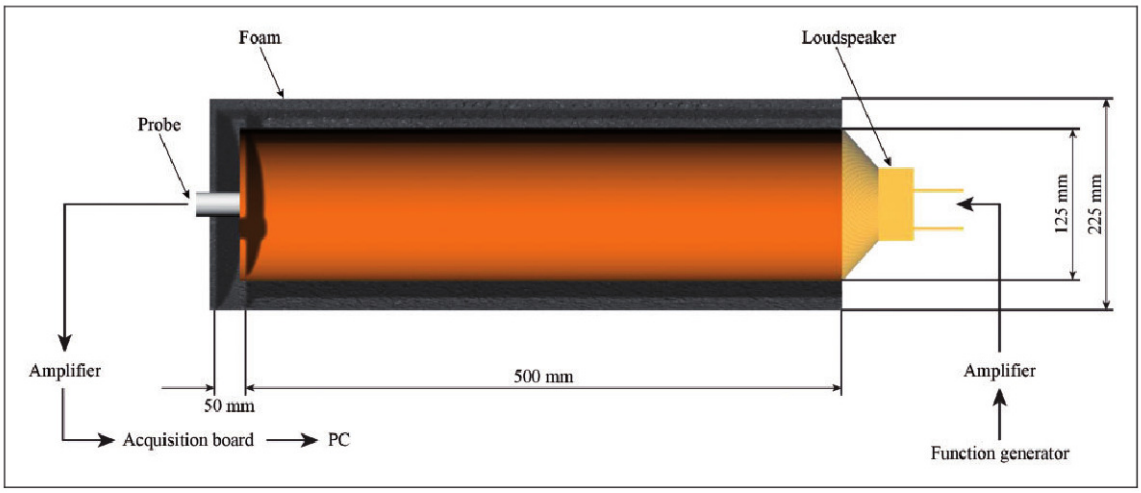

Figure 5. Characterisation test-rig.

according to requirements. The frequencies used are the typical ones for the axial fan available for the authors. The function generator technical parameters are listed in Table 4.

Signal amplifier

A signal amplifier has been placed between the function generator and the loudspeaker in order to compensate for the loudspeaker's low impedance and to avoid damage in the function generator. The amplifier circuit used is based on a TDA2003, capable of delivering 4 Wrms at 4 Ω, and it is designed to operate with the specifications in the following Table 5. The integrated circuit is thermally and short-circuit protected. Figure 6 shows the amplifier circuit.

Axial fan test-rig

Axial fan specification

The turbomachine used for the experimental tests is a low-speed industrial fan. Table 6 shows the specifications for the fan.

A 1.55 kW direct coupled-induction three-phase motor was used to drive the rotor at a constant speed of 1000 r/min. Under these circumstances the blade passage frequency (BPF) for the tested configuration was 100 Hz, and the rotor frequency 16 Hz. The test-rig airway is set according to the type-D configuration ISO 5801:2007.[17] The fan was driven to stall by throttling at the upstream end of the duct.

Instrumentation set-up

The fan rotor casing was instrumented with two inserts containing a pressure transducer and a dynamic microphone. The piezoelectric microphone was placed at 1 m distance from the fan casing, normal to the fan rotor. The probe arrangement is illustrated in Figure 7.

The tests sampling time interval was 60 s with a sample frequency of 24 kHz, which is the acquisition board limit. In order to have significant acquired signals, it is been necessary to amplify the instruments. The experimental procedure was to provide a reduction of the flow rate through a throttle upstream the rotor, starting from a stable work condition until reaching the rotating stall.

Table 5. Signal amplifier specifications.

Output power	7 W / 4 Ω
RMS output power	3.5 W / 4 Ω or 2 W / 8 Ω
Total harmonic distortion	0.05% (1 W / 1 kHz)
Frequency response	20 Hz to 20 kHz (−3 dB)
Input sensitivity	40 mV / 150 kΩ
Signal-to-noise ratio	86 dB (A weighted)
Power supply	8–18 VDC / 0.5 A
Dimensions	55 × 35 mm^2 (2.2" × 1.4")

Table 6. Fan data.

Nominal speed	1000 r/min
Tip speed	40.6 m/s
Internal duct diameter	800 mm
Blade count	6
Blade length	200 mm
Tip clearance	5 mm
Blade chord at the tip	125 mm

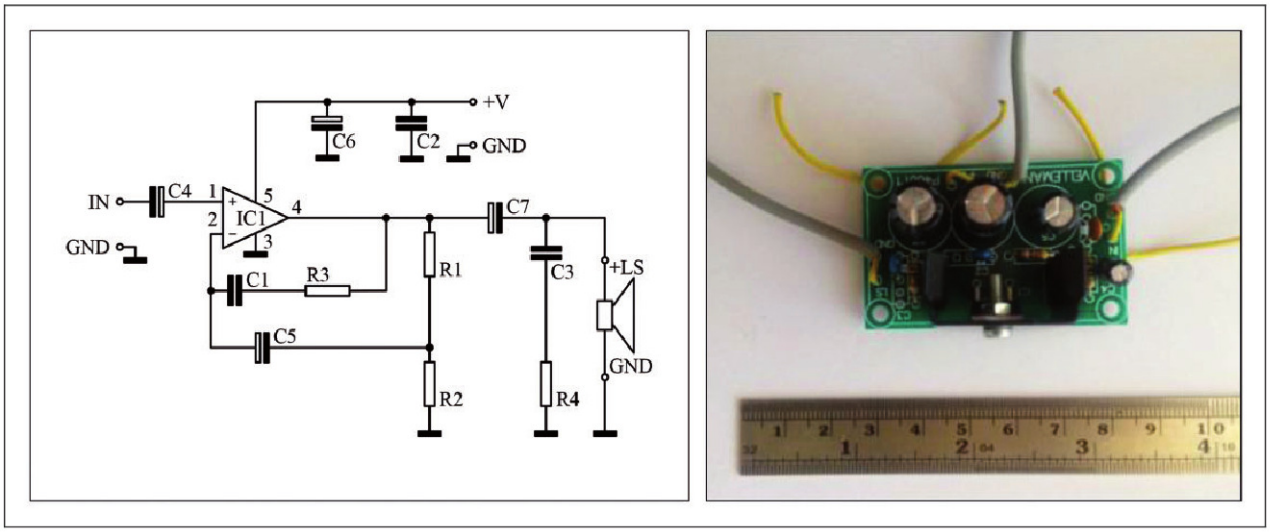

Figure 6. The amplifier circuit.

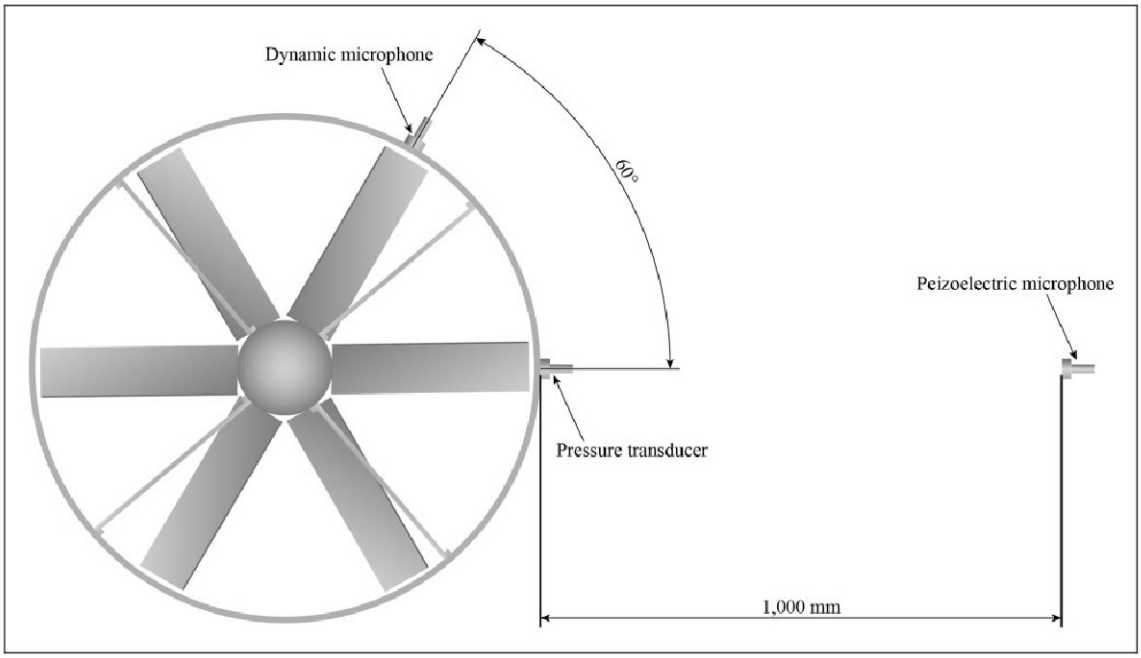

Figure 7. Location of the sensors.

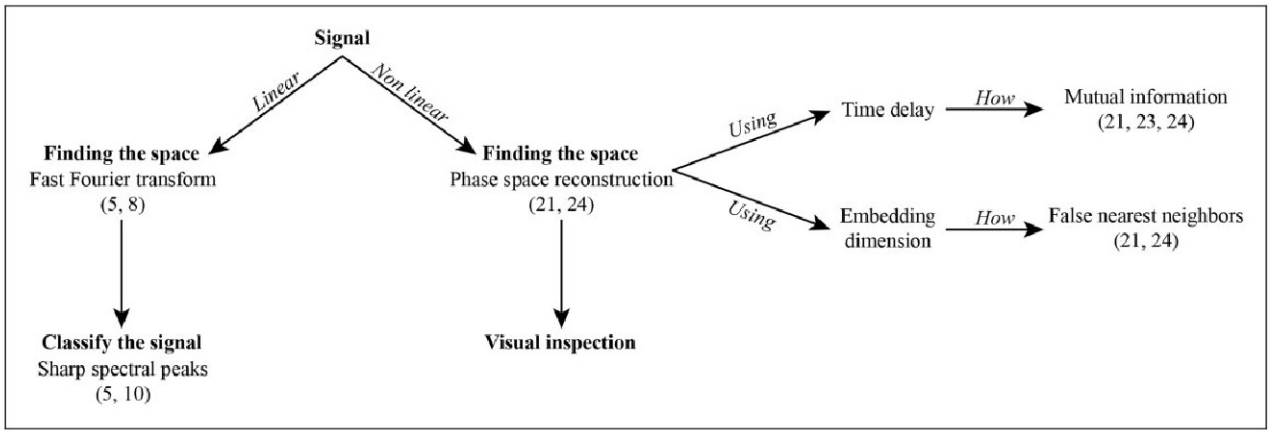

Figure 8. Outline used for the signal analysis.

Signal processing

Figure 8 describes the methods used for the signal analysis, distinguishing between linear and non linear signal processing. Both methods have the same purpose, although the techniques are very different.

The analysis performed on the acquired signals are the visual inspection on the filtered signals in the time domain, and a signal processing that includes a frequency-domain analysis based on fast Fourier transform (FFT), and a time-domain analysis based on the reconstructed phase space (RPS) portraits.

The spectral analysis provides information about the power distribution over the frequency. The FFT is implemented to evaluate the spectrum of a temporal signal. The time signal is discrete depending on the acquisition sample rate. The authors inspected the pressure signals through the spectral analysis in order to identify the frequency bands that reveal the rotating stall occurrence, as in the cross-correlation analysis already developed by Park.[18]

The time-domain signal analysis was based on the RPS, following the stall detection through acoustic methods already investigated in Bianchi et al.[19] which proposed the use of symmetrised dot pattern representation of pressure sound signals in order to differentiate between critical and noncritical stall conditions, and to identify stall precursors. Also, Palomba et al.[20] studied the chaotic dynamics on which the rotating stall is based. They reconstructed the phase space portraits of velocity, static pressure

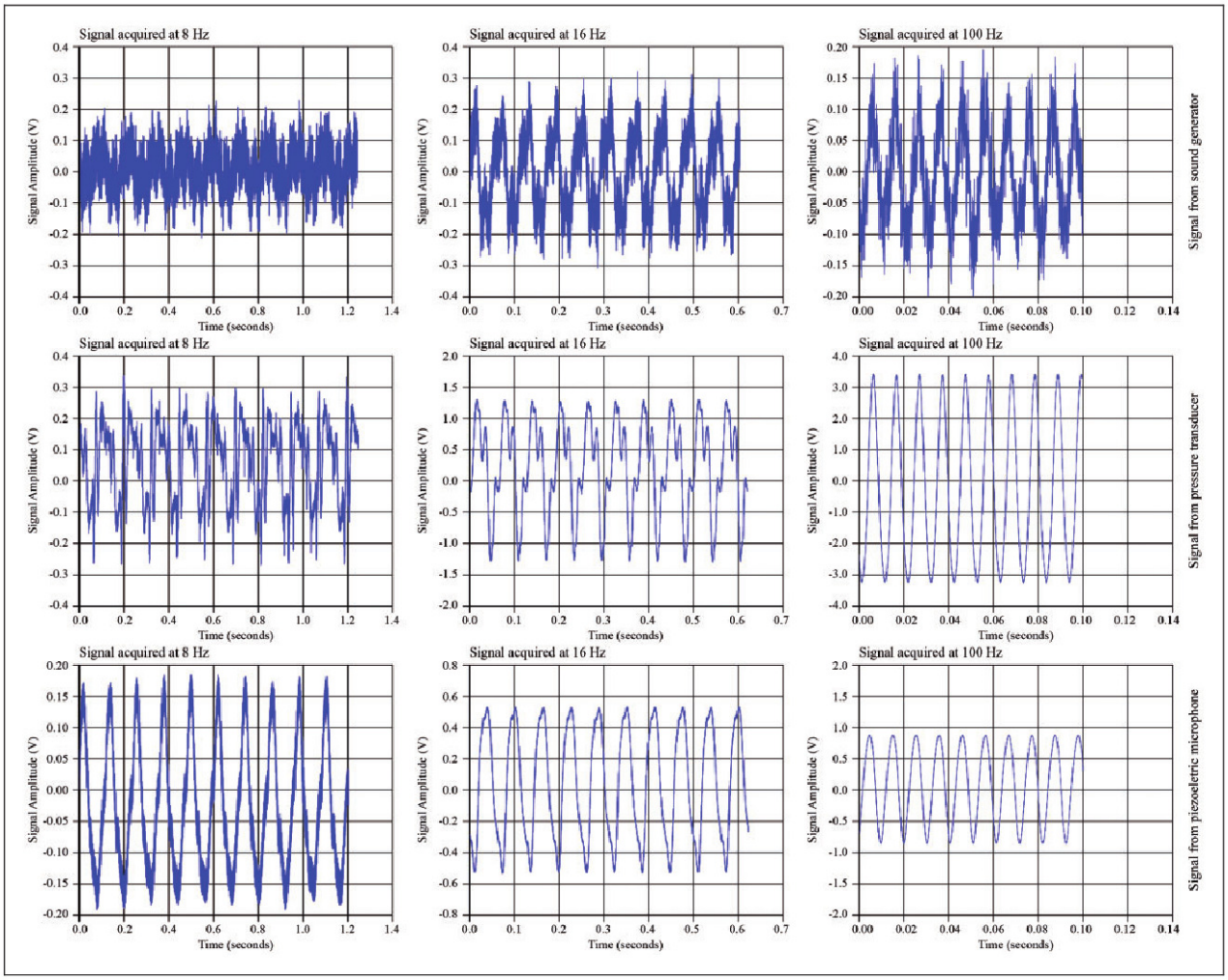

Figure 9. Sound generator signals acquired at 8 Hz, 16 Hz, 100 Hz, with the pressure transducer (a), the dynamic microphone (b) and the piezoelectric microphone (c).

Table 7. Periods and time delay used in the investigation.

Frequency (Hz)	Period (s)	Time delay T		
		Pressure	Dynamic	Piezoelectric
8	1.25	2	1	2
16	0.625	6	2	2
100	0.1	6	5	5

and vibration experimental signals data series, using the delay method. Their idea was to represent the system dynamics and the transient phenomena using a non linear tool, on the basis of patterns identification and trajectories inspection.

With the phase space reconstruction it is possible to do the embedding of a univariate sequence of data (the signal considered as a time series) in a RPS evaluating the time lag T and the embedding dimension D, so to obtain $\mathbf{D}$ vectors from the original signals using T as the time delay.[21] The RPS representation reads as

$$\begin{bmatrix} x_1 \\ x_2 \\ \vdots \\ x_t \\ \vdots \\ x_{N-(D-1)T} \end{bmatrix} = \begin{bmatrix} x_1 & x_{1+\tau} & \cdots & x_{1+(D-1)\tau} \\ x_2 & x_{2+\tau} & \cdots & x_{2+(D-1)\tau} \\ \vdots & \vdots & \ddots & \vdots \\ x_t & x_{t+\tau} & \cdots & x_{t+(D-1)\tau} \\ \vdots & \vdots & \ddots & \vdots \\ x_{N-(D-1)T} & x_{N-(D-2)T} & \cdots & x_N \end{bmatrix} \quad (1)$$

The RPS allows the identification of the characteristics contained in the nonlinear dynamic systems, which are not identifiable with the time domain

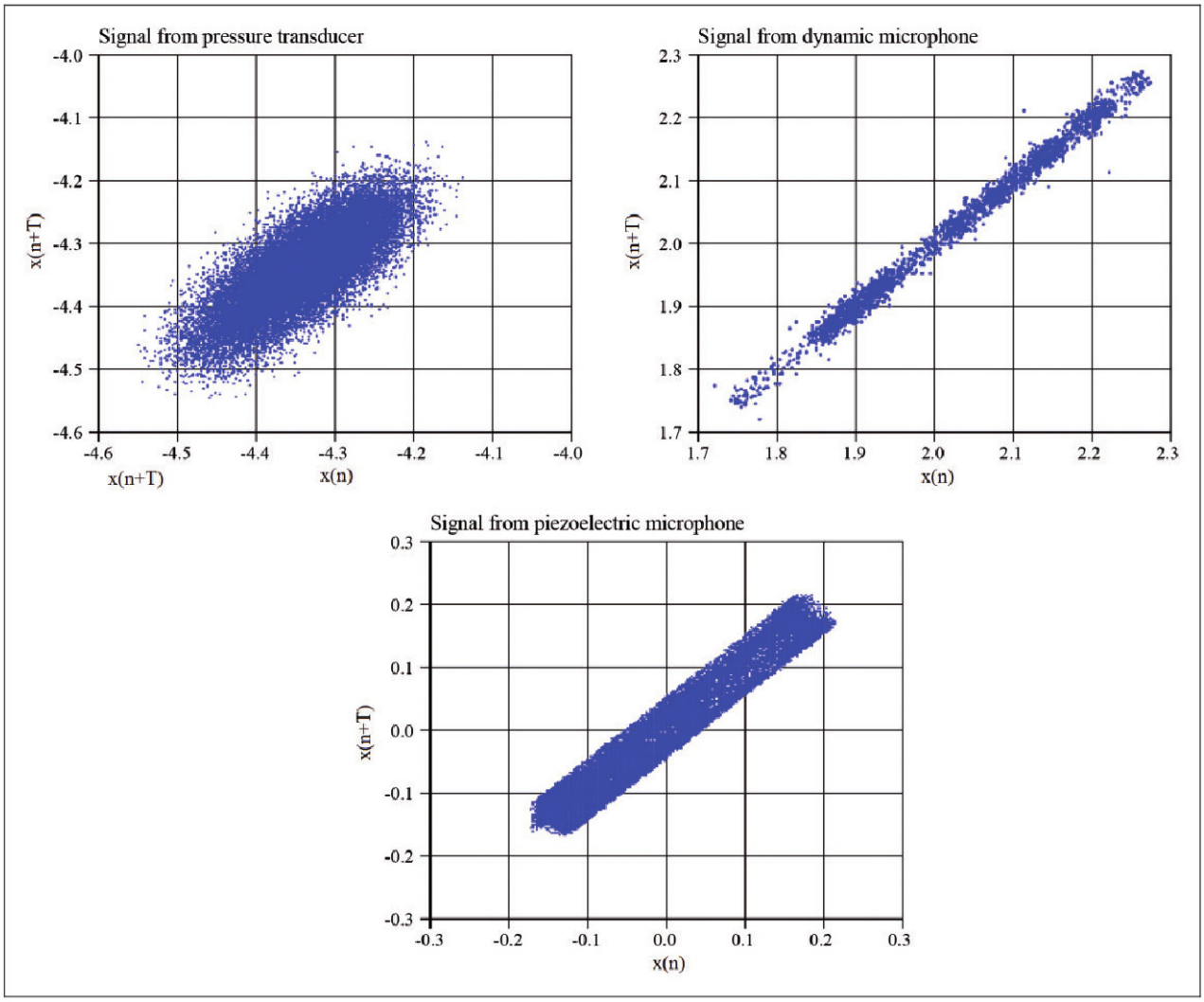

Figure 10. RPS at 8 Hz for: (a) pressure transducer, (b) dynamic microphone, (c) piezoelectric microphone.

analysis of the single signal, as already shown in Corsini et al.[22] The accurate reconstruction of the phase space depends on the definition of D and T. The optimal time delay T is identifiable with the first minimum of the mutual information,[23] while the embedding dimension D is identifiable with the false nearest neighbours method.[24] The used value of D is 2 in every case, meaning that the dynamic system is observable in a two-dimensional space, where the two dimensions are the most important ones between the infinite possible dimensions; moreover, increasing the embedding dimension D does not result in an increase of information.

Results

Probe characterisation by visual inspection

Figure 9(a) to (c) illustrates the visual inspection of the signals acquired in the characterization test-rig, respectively with the pressure transducer, the dynamic microphone and the piezoelectric microphone. The sinusoidal signals were acquired at the three most representative frequencies for the axial fan, namely the rotating stall frequency 8 Hz, the rotor frequency 16 Hz and the BPF 100 Hz, with a sample frequency f_S of 24 kHz, corresponding to the Nyquist frequency $f_N = f_S/2 = 12$ kHz.

The comparative visual inspection demonstrates that the pressure transducer gives a disturbed signal at very low frequencies as well at the higher ones. The dynamic microphone signals show a behaviour very comparable to the piezoelectric microphone ones mainly at the higher frequency, and they are able to reconstruct the sinusoidal response even at the lowest frequency, that is 8 Hz in the test. In contrast the reference probe, clearly, outperforms the two DIY technologies with small distortions at the low frequencies.

Probe characterisation by RPS portraits

The values of T used, in the present investigation, are summarised in Table 7. Notably, the indicated periods are representative of 10 signal oscillations for each of the analysed frequencies.

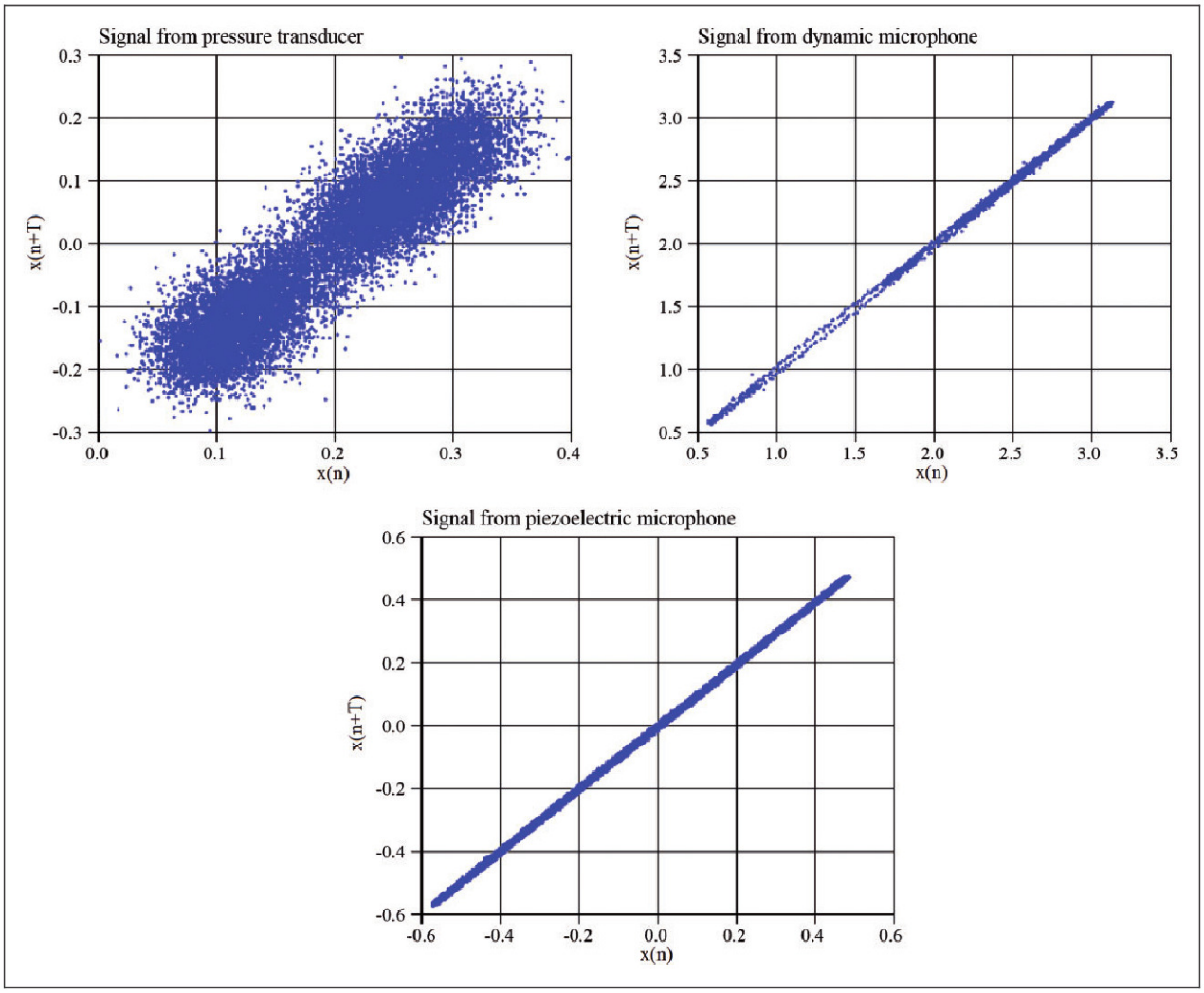

Figure 11. RPS at 16 Hz for: (a) pressure transducer, (b) dynamic microphone, (c) piezoelectric microphone.

Figure 10 shows the RPS patterns at the frequency of 8 Hz, for the signal acquired with the pressure transducer, the dynamic microphone and the piezoelectric microphone respectively. The period considered corresponds to a time interval of 1.25 s, corresponding to 10 signal oscillations.

Figure 11 shows the RPS patterns at the frequency of 16 Hz, for the signal acquired with the pressure transducer, the dynamic microphone and the piezoelectric microphone respectively. The period considered corresponds to a time interval of 0.625 s, corresponding to 10 signal oscillations.

Figure 12 shows the RPS patterns at the frequency of 100 Hz, for the signal acquired with the pressure transducer, the dynamic microphone and the piezoelectric microphone respectively. The period considered corresponds to a time interval of 0.1 s, corresponding to 10 signal oscillations.

The RPS portraits comparison indicates that the methodology is able to precisely identify the pure frequencies of interest for the later axial fan analysis. The patterns diagonal stretching, indicates the predominance of a punctual frequency. The pressure transducer results to be the less precise between the sensors used, showing more disorderly patterns, while comparing the responses of the dynamic microphone and the piezoelectric microphone used as a base line, they show a very similar behaviour.

Axial fan analysis

The pressure signals have been acquired at a sample frequency f_S of 24 kHz, corresponding to a Nyquist frequency f_N of 12 kHz.

Figure 13 shows the signals acquired with the two near-field sensors and the far-field microphone. Figure 13(a) and (b) represents the signal time traces measured by the pressure sensor and the dynamic microphone respectively, while Figure 13(c) illustrates the signal time trace measured through the reference piezoelectric microphone.

The spectral and the RPS analyses have been applied over a time window of 1 s, equivalent to approximately 16 rotor revolutions, selecting operating conditions

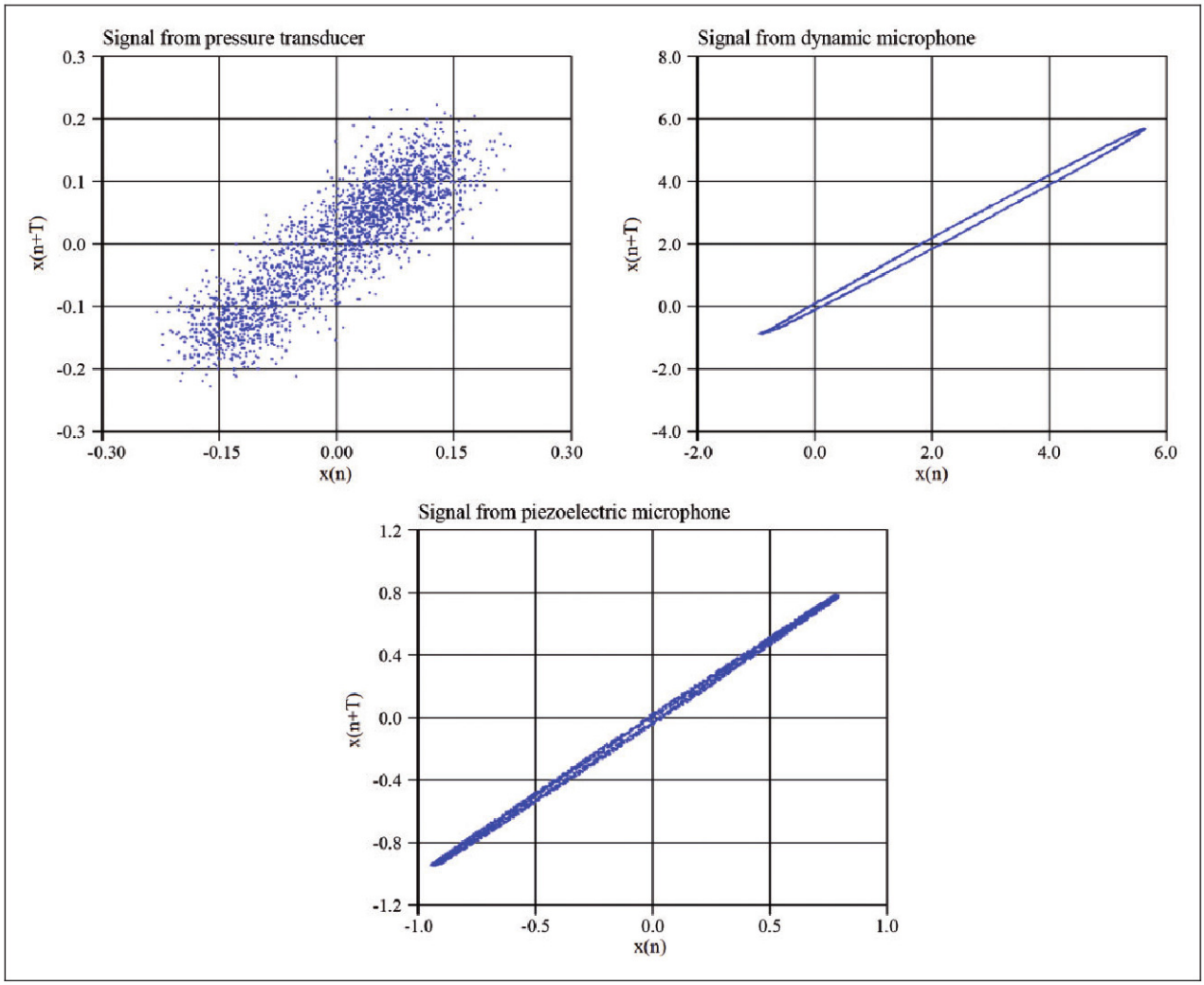

Figure 12. RPS at 100 Hz for: (a) pressure transducer, (b) dynamic microphone, (c) piezoelectric microphone.

which are representative of stable and stalled operations. The time windows have been taken in the steady and in the unsteady region of the acquired signals.

Moreover, Figure 14 illustrates the auto-spectra of the signals measured by the pressure transducer (Figure 14(a)), the dynamic microphone (Figure 14(b)) and the piezoelectric microphone (Figure 14(c)) during the stable and stalled work condition.

When looking at the DIY probes spectra, it is remarkable that their response in the frequency range above the first harmonic of the BPF is attenuated. This circumstance is in general true at stable operations for the DIY spectra, and it applies also with the fan operated at stall. In this condition, the DIY sensors appeared to give rise to a much richer spectral signature but in the limit of the low frequency range, that is much affected by the emergence of rotating instability tones, such as stall, at about 50% of the rotor frequency (i.e. 16 Hz for the tested fan). In this respect the far-field piezoelectric probe used as a baseline, is able to resolve all the frequency components in the sound radiated from the test-tube in a fully reverberant environment.

Axial fan phase-space portraits RPS

The values of T used, in the investigation about the axial fan, are summarised in Table 8. Notably, the indicated periods are representative of 1 s for each of the analysed time windows.

Figure 15 shows the evolution of the RPS in a stable operating condition and during the aerodynamic instability for the signal acquired with the pressure transducer. The stable condition corresponds to the time interval 1–2 s, the stalled condition correspond to the time interval 45–46 s of the signal in Figure 13(a).

Figure 16 shows the evolution of the RPS starting from a stable operating condition towards the aerodynamic instability for the signal acquired with the dynamic microphone in the time intervals highlighted in Figure 13(b).

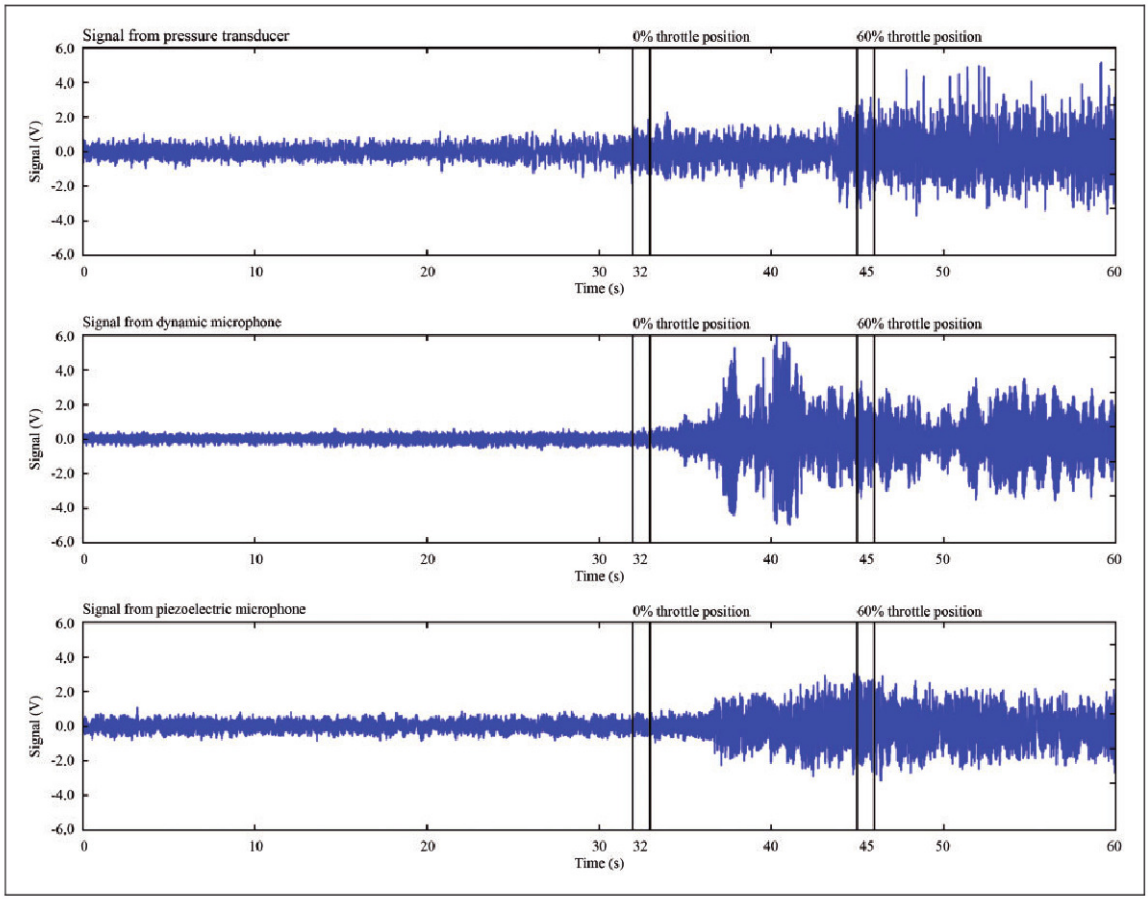

Figure 13. The axial fan acquired signals in time domain for: (a) the pressure transducer, (b) the dynamic microphone, (c) the piezoelectric microphone.

Concerning the piezoelectric microphone, it was placed in the far field at 1 m from the fan casing as shown in Figure 7. Figure 17 shows the evolution of the RPS starting from a stable operating condition towards the aerodynamic instability for the signal acquired with the piezoelectric microphone for the time intervals highlighted in Figure 13(c).

Notably, in addition to the evidence of the spectral analysis, the portrait comparison indicates that both the signals from the pressure transducer and the dynamic microphone are able to create phase-space patterns which identify sharply the evolution from stable to stalled operations. The signature of such evolution being the diagonal stretching of patterns and, as already explained, this circumstance could be correlated with the predominance at stall of a given frequency and a chaotic behaviour with the orbits of RPS attractor evolving in a complex shape; whereby some directions are contracted and other are stretched.

Conclusions

From the frequency domain analysis through the FFT is noticeable that rotating stall occurs at low frequencies, lower than 100 Hz; more importantly the rotating stall is visible with both the DIY instruments. The clearly visible frequency peak at 64 Hz during stalled operations is considered to be a resonant frequency due to the rotor–stator interaction. The experiment proves that the dynamic microphone is able to detect the presence of aerodynamic instabilities at frequencies lower than 20 Hz with a 50–60% precision. Indeed applying the spectral analysis on the dynamic microphone signal, it is possible to detect a peak at about 15 Hz which is near the value 16.2 Hz of the rotor frequency. Using the RPS method the authors identified the typical rotating stall pattern. As in the spectral analysis, the method response is more chaotic, and the pattern tends to enlarge and extend while approaching the unsteady condition.

Both the pressure transducer and the dynamic microphone have detected the presence of the rotating stall phenomenon, and the analysis methods used confirmed the validity of the used instruments.

However, from the RPS analysis of the sine wave signals, it is especially evident for the lower frequency, how the dynamic microphone works better than the pressure transducer, if the piezoelectric microphone is taken as a reference. And this is confirmed in the RPS

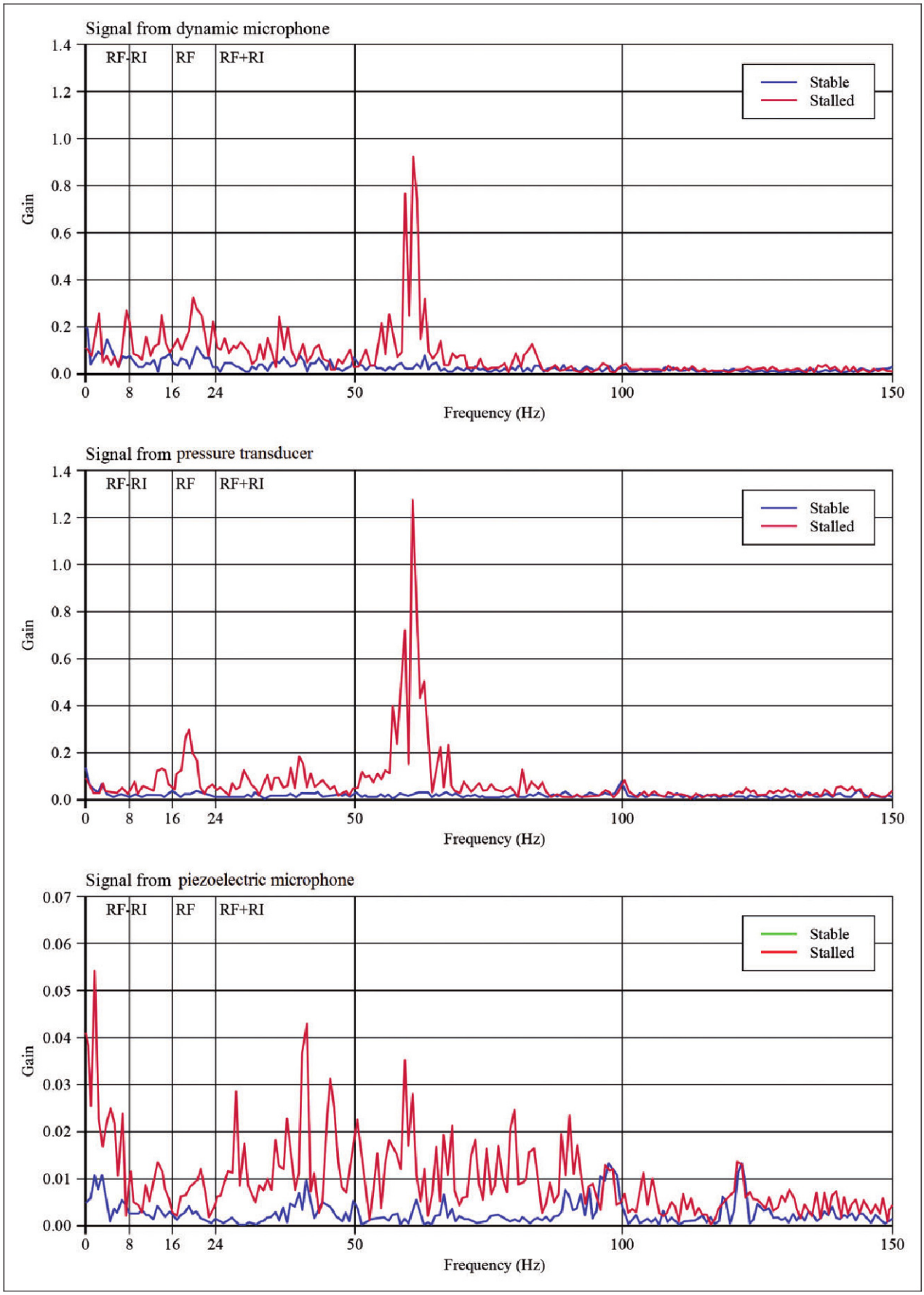

Figure 14. Spectral analysis for stable and stalled signals of: (a) pressure transducer, (b) dynamic microphone, (c) piezoelectric microphone.

Table 8. Used *T* values.

Period (s)	Time delay *T*		
	Pressure	Dynamic	Piezoelectric
1–2	5	5	10
45–46	8	7	2

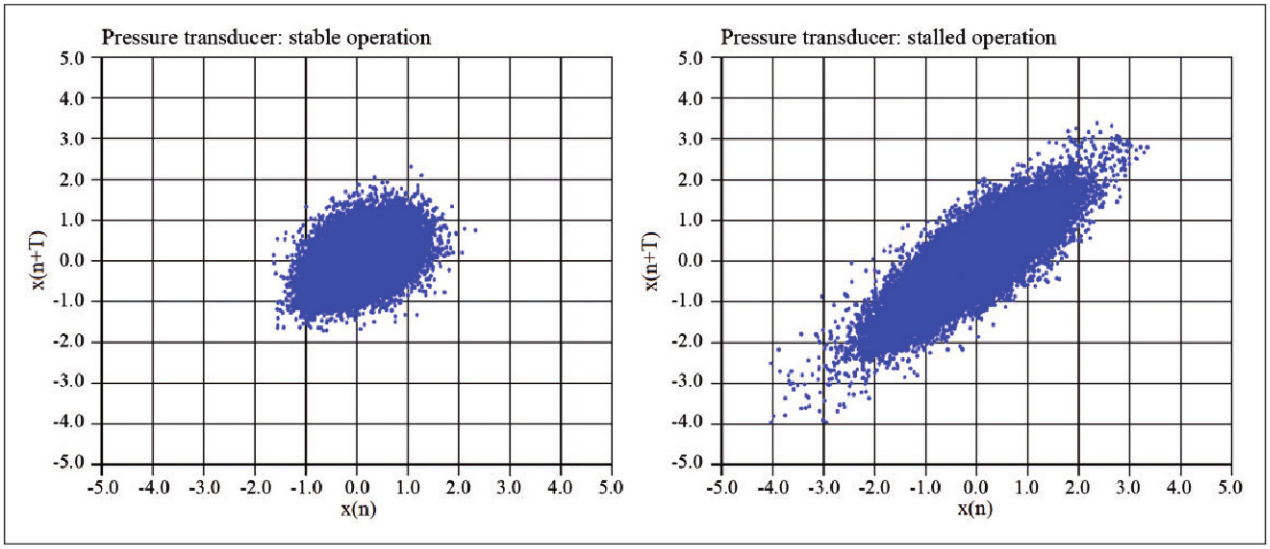

Figure 15. On the left the stable operation, on the right the stalled operation for the pressure transducer.

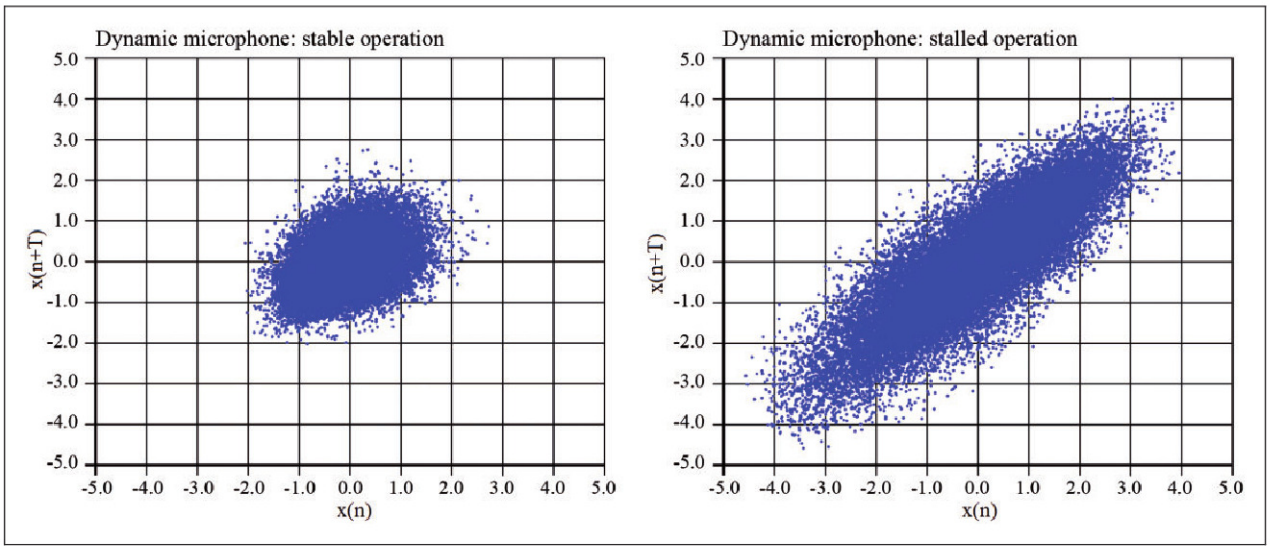

Figure 16. On the left the stable operation, on the right the stalled operation for the dynamic microphone.

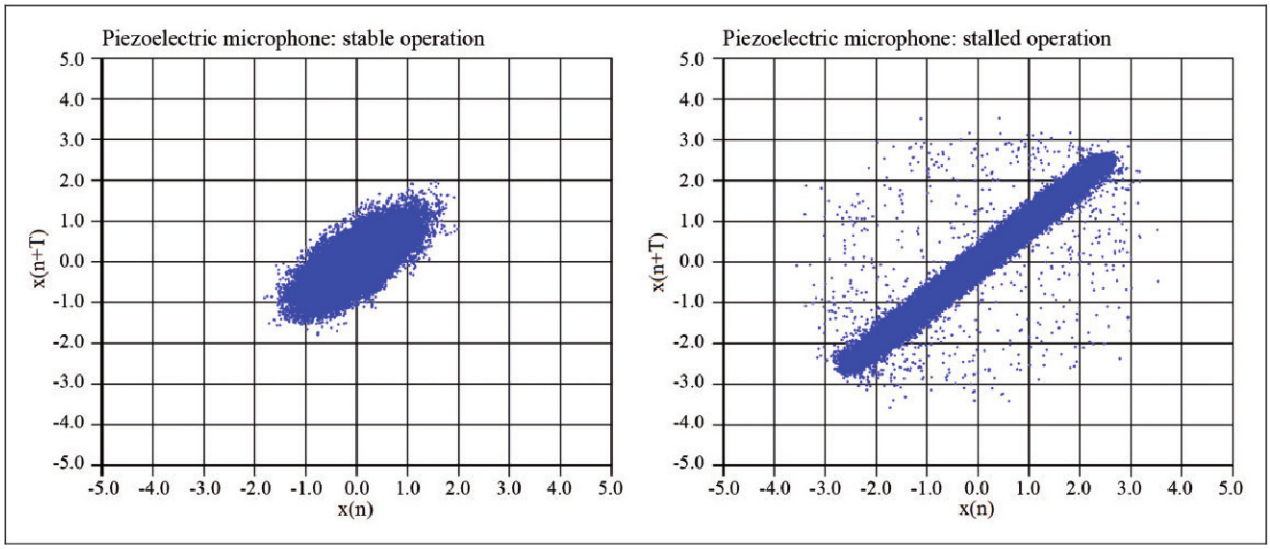

Figure 17. On the left the stable operation, on the right the stalled operation for the piezoelectric microphone.

analysis, where the similarity between the dynamic and piezoelectric microphone system response is visible.

Declaration of conflicting interests

The author(s) declared no potential conflicts of interest with respect to the research, authorship, and/or publication of this article.

Funding

The author(s) received no financial support for the research, authorship, and/or publication of this article.

References

1. Emmons HW, Pearson CE and Grant HP. Compressor surge and stall propagation. *Trans ASME* 1955; 77: 455–469.
2. Greitzer EM. Review - Axial compressor stall phenomena. *J Fluids Eng* 1980; 102: 134–151.
3. Day IJ and Cumpsty NA. The measurement and interpretation of flow within rotating stall cells in axial compressors. *J Mech Eng Sci* 1978; 20: 101–114.
4. Moore FK. A theory of rotating stall of multistage compressors (parts I–III). *ASME J Eng Power* 1984; 106: 313–336.
5. Tan CS, Day I, Morris S, et al. Spike-type compressor stall inception, detection, and control. *Ann Rev Fluid Mech* 2010; 42: 275–300.
6. Bianchi S, Corsini A, Sheard AG, et al. A critical review of stall control techniques in industrial fans. *ISRN Mech Eng* 2013; 2013. Article ID 526192, 18pp.
7. Stone A. Effects of stage characteristics and matching on axial-flow-compressor performance. *Trans ASME* 1958; 80: 1273–1293.
8. Cumpsty NA. A critical review of turbomachinery noise. *J Fluids Eng* 1977; 99: 278–293.
9. Cumpsty NA. Sum and difference tones from turbomachines. *J Sound Vib* 1974; 32: 383–386.
10. Bianchi S, Corsini A, Mazzucco L, et al. Stall inception, evolution and control in a low speed axial fan with variable pitch in motion. *J Eng Gas Turbines Power* 2012; 134042602-1.
11. Bianchi S, Corsini A and Sheard AG. Detection of stall regions in a low-speed axial fan. Part I - Azimuthal acoustic measurements. In: *Proceedings of ASME*, GT2010-22753, 2010.
12. Zhu T and Carolus TH. Experimental and unsteady numerical investigation of the tip clearance noise of an axial fan. In: *ASME Turbo Expo 2013: Turbine Technical Conference and Exposition*, San Antonio, Texas, USA, 3–7 June 2013, Paper No. GT2013-94100, pp. V004T10A001, 12.
13. Bennett GJ, Mahon J, Hunt S, et al. Design of an electret based measurement microphone. In: *26th international manufacturing conference (IMC26)*, Dublin, Ireland, 2–4 September 2009, pp.411–418.
14. Bianchi S, Corsini A and Sheard AG. Experiments on the use of SDP for in-service stall detection in industrial fans. In: *Fan 2012*, Senlis, France, 18–20 April 2012.
15. Corsini A, Feudo S, Tortora C, et al. Stall detection using near-field low frequency and pressure modulation in turbomachines. In: *Inter-noise 2014*, Melbourne, Australia, 16–19 November 2014.
16. Louw FG, Von Backström TW and Van Der Spuy SJ. Experimental investigation of the blade surface pressure distribution in an axial flow fan for a range of flow rates. In: *ASME turbo expo*, Montreal, Canada, 15–19 June 2015, GT2015-43620.
17. ISO 5801. Industrial fans—Performance testing using standardized airways, 2007.
18. Park HG. *Unsteady disturbance structures in axial flow compressor stall inception*. MS Thesis, Massachusetts Institute of Technology, Cambridge, MA, USA, 1994.
19. Bianchi S, Corsini A and Sheard AG. Demonstration of a stall detection system for induced-draft fans. *J Power Energy* 2013; 227: 272–284.
20. Breugelmans FAE, Palomba C and Funk T. Application of strange attractors to the problem of rotating stall. In: Y Tanida and M Namba (eds) *Unsteady aerodynamics and aeroelasticity in turbomachinery*. New York: Elsevier Science, 1995.

21. Abarbanel HDI, Brown R, Sidorowich JJ, et al. The analysis of observed data in physical systems. *Rev Mod Phys* 1993; 65: 1343–1351.
22. Corsini A, Feudo S, Sheard AG, et al. Implementation of an acoustic stall detection system using near-field DIY pressure sensors. In: *Fan 2015*, Lyon, France, 15–17 April 2015.
23. Gallager R. *Information theory and reliable communication*. New York: John Wiley and Sons, 1968.
24. Kennel MB, Brown R and Abarbanel HDI. Determining embedding dimension for phase space reconstruction using a geometrical construction. *Phys Rev A* 1992; 45: 3403–3411.

Appendix

Notation

n	index of row vortex
Q	embedding dimension
T	time delay
$x(n)$	scalar time series
$x(n+T)$	lagged scalar time series